Journal of Sustainable Development of Energy, Water and Environment Systems

http://www.sdewes.org/jsdewes

Year 2025, Volume 13, Issue 3, 1130578

Original Research Article

Numerical Simulation of Co-combustion of Solid Recovered Fuel in Cement Kiln Installation

Grzegorz Borsuk[1], Jacek Wydrych[1], Małgorzata Wzorek[*2], Ewa Głodek-Bucyk[3], Pavlos Zalimidis[4]

[1]Department of Thermal Engineering and Industrial Facilities,
Opole University of Technology, Opole, Poland
e-mail: g.borsuk@po.edu.pl; j.wydrych@po.edu.pl

[2]Department of Process and Environmental Engineering,
Opole University of Technology, Opole, Poland
e-mail: m.wzorek@po.edu.pl

[3]Łukasiewicz Research Network – Institute of Ceramics and Building Materials,
Opole, Poland
e-mail: ewa.glodek-bucyk@icimb.lukasiewicz.gov.pl

[4]ASPETE School of Pedagogical and Technological Education – Department of Mechanical Engineering Educators Athens, Greece
e–mail: pzalimidis@aspete.gr

Cite as: Borsuk, G., Wydrych, J., Wzorek, M., Głodek-Bucyk, E., Zalimidis, P., Numerical Simulation of co-combustion of Solid Recovered Fuel in Cement Kiln Installation, J.sustain. dev. energy water environ. syst., 13(3), 1130578, 2025,
DOI: https://doi.org/10.13044/j.sdewes.d13.0578

ABSTRACT

The study aim was to determine the technical parameters of Solid Recovered Fuel (SRF) fuel inlet into the Air Through precalciner (AT-type) while maintaining process stability and the quality characteristics of the produced cement clinker. The simulation was done for a real-scale plant using numerical Computer Fluid Dynamics (CFD) modelling with the use of own developed calculation method. The method enables consideration of the primary effects of combustion, identification of process changes trends, and incorporation of particulate matter from SRF fuel and raw meal into process stability. The model was based on Eulerian–Lagrange two phase flow approach. The processes occurring in the decarbonization zone are modelled using a simplified one-dimensional approach. Based on the conducted research, the optimal location for the Solid Recovered Fuel fuel inlet was determined with a fuel inlet diameter of 150 mm, a fuel flow rate of 1000 kg/h, and a transport air flow rate of 1000 Nm^3/h.

KEYWORDS

Solid recovered fuel, Co-combustion, Cement rotary kiln, Air through precalciner, Computer Fluid Dynamics (CFD) modelling.

INTRODUCTION

The cement industry ranks as the third-largest industrial energy consumer, accounting for 7% of global industrial energy usage (10.7 EJ) and contributing to 7% of total CO_2 emission [1].

* Corresponding author

The extent of substitution of fossil fuels with alternative fuels derived from waste in cement production varies significantly across different regions of the world. In European Union countries, including Poland, the co-combustion of alternative fuels in rotary kilns for clinker production has already reached a very high level. In 2021, the share of alternative fuels in cement plants in Poland reached 75%, with some individual cases surpassing even 90%, while the European Union average was 54% [2]. In quantitative terms, this corresponded to the use of 1.666 million tons of alternative fuels annually in Poland, and 12.9 million tons across Europe [3]. RDF/SRF fuels represent the largest group of fuels used by the cement industry, accounting for 34% of the total alternative fuels consumed in 2021.

Both RDF and SRF are produced from the non-hazardous fraction of municipal solid waste (MSW). However, SRF follows a standardized production procedure, and its quality parameters are defined and classified according to an established international standard set by the CEN/TC 343 technical committee [4]. The SRF classification process incorporates limit values for three key fuel characteristics: net calorific value (NCV), chlorine content (Cl), and mercury content (Hg). Each of these characteristics is divided into five classes based on the values of NCV, Cl content, and Hg content. As the class number increases, the quality of the SRF decreases. The SRF class code is ultimately determined by the combination of these three individual class values. A consistent quality standard and reliable quality assurance are required when SRF is used for energy recovery in cement plants.

To provide the energy required for the clinker phase transition, different types of fossil and alternative fuels are commonly burned through the main burner- multi-channel burners in the rotary kiln but also via different types of precalcinators.

The diversity of types of alternative fuels used, the extent of their utilization, and the methods of their introduction into the kiln in each case necessitate an individual approach in determining the technological conditions needed for their use [5] [6].

The mechanism of burning alternative fuels differs from that of fossil fuels [7]. It is a heterogeneous process, stemming from the diversity of composition, variability in physicochemical characteristics of fuel components, and properties of combustible fraction, as well as the level of O_2 concentration in gases introduced into the kiln.

Additionally, the ash resulting from the combustion of alternative fuels undergoes complete absorption in the clinker, which necessitates considering its composition as a raw material component determining the chemical and phase composition of the clinker [8].
Moreover, alternative fuels have large, non-spherical particles which are differ from particles derived from conventional fossil fuels, and in simplified terms, can be considered as point masses [9]. Consequently, employing specific numerical models of particle movement can be advantageous in modeling the combustion process of alternative fuels.

With the advancement of computational fluid dynamics (CFD) methods, numerical simulations have become increasingly prevalent in the design and optimization of industrial processes. In some works, numerical modeling was extended to include aspects of the combustion process [10] [11], chemical transformations and the rotational motion of the cement kiln [12] was taken into account. Given the intricate conditions within the cement rotary kiln, which involve gas-solid two-phase flow and heat transfer, CFD modeling has emerged as an indispensable tool to support processes related to cement production.

Numerous studies have explored the impact of co-combustion various alternative fuels on the burning process, temperature profiles, interaction with the clinker bed, and kiln corrosion in the rotary kiln. Hercog *et al.* [13] conducted experimental and numerical studies on the co-combustion of petcoke with alternative fuels in a 1 MW multifuel burner and demonstrated that it is possible to achieve a substitution rate of up to 100% using biomass or RDF (SRF) without significantly affecting combustion efficiency. However, at high RDF shares (≥80% of energy), a slight shift of the flame front and flame elongation was observed, which may affect heat transfer in the clinker sintering zone and combustion efficiency. Meanwhile, Pieper et al.

[5] used CFD modeling to analyze coal combustion with RDF in a rotary kiln and found that co-combustion of RDF may lead to a reduction in gas and clinker temperatures in the sintering zone, which could impact clinker properties. Ariyaratne *et al.* [14] investigated the effect of fuel feeding position and particle size on combustion characteristics in CFD simulations of meat and bone meal (MBM) and coal combustion in a cement kiln. The study found that annulus fuel feeding, compared to central-tube feeding, allows better dispersion of larger fuel particles across the kiln cross-section, improving mixing with oxygen and enhancing combustion efficiency.

However, there is relatively limited information regarding the co-combustion of alternative fuels in precalciners, especially in Air Through (AT-type) precalciners. In this type of precalciner alternative fuels are introduced into the AT-type precalciner between the cyclone preheater tower and the rotary kiln under different process and temperature conditions compared to the cement kiln. It is state that the degree of raw material calcination is directly dependent on the amount of fuel burned in the precalciner and is influenced by multiple parameters, including thermal conditions within the system, material residence time, dust concentration, dust circulation, and the kinetics of chemical reactions. The complexity of these interdependent mechanisms necessitates the application of computational fluid dynamics (CFD) simulations to achieve a precise analysis of the process.

The parameters of solid particles conveying are very important, which affect the separation between the upper and lower sections of the AT-type precalciner. Chen *et al.* [15] described the calculation methodology for solid particles of ground concrete in a horizontal pipeline. The basic process in the AT-type precalciner is the calcination process, which requires appropriate temperature conditions. Kang *et al.* [10], presented the method of calculating the degree of calcination based on DEM-CFD coupled simulation. Reineking *et al.* [16] showed the results of numerical calculations of gas movement for the wood chips drying process using coupled DEM-CFD simulations. Gao *et al.* [17] argue that existing research is insufficient to provide a comprehensive understanding of the processes in this region of kiln installation. Attention should be paid to the impact of waste addition on its combustion characteristics, the rate of raw material decomposition, and the generation and reduction of NO_x in the precalciner. Zhang *et al.* [18] proposed to reduce NO_x in the cement precalciner by ammonia injection in the high-temperature and lean-oxygen zone during pulverized coal combustion.

Mikulcic *et al.* [19] focused on the fundamental equations of continuum mechanics, emphasizing mass, momentum, and energy conservation laws but did not account for variations in particle size during calcination. Similarly, Leyu *et al.* [20] applied the CFD method to simulate pulverized coal gasifiers, incorporating the discrete phase model (DPM) to track coal particles and using the Rosin–Rammler distribution for particle size representation. However, these simulations assumed a constant particle size throughout the process. Furthermore, the study on CFD simulation of a cement precalciner with agglomerate-based drag modeling employed a two-fluid model in ANSYS Fluent but maintained fixed particle properties, including density and heat capacity [21].

Unlike previous works, our study introduces a novel approach by incorporating the dynamic change in particle diameter and mass during calcination, which significantly impacts heat and mass transfer phenomena. This modification enhances the accuracy of numerical predictions by capturing the real-time effects of particle shrinkage on reaction kinetics and fluid dynamics. By integrating this aspect into the CFD framework, our research provides a more comprehensive understanding of the calcination process, contributing to the optimization of cement production efficiency and sustainability. To perform these calculations, additional user-defined functions (UDF) were created and implemented into the ANSUS-Fluent.

Furthermore, although combustion and calcination processes in cement kilns have been extensively studied using various numerical models, the specific impact of SRF fuel inlet

positioning within the riser duct has not been systematically investigated. This study addresses this research gap by analyzing how fuel inlet placement influences combustion dynamics and calcination efficiency. By minimizing reliance on experimental trial runs, the proposed approach enhances numerical modeling accuracy and provides valuable data for optimizing process control in cement production.

This study was conducted on an industrial-scale cement plant utilizing CFD simulations incorporating a newly developed calculation methodology. The proposed modeling framework enabled a detailed assessment of physicochemical phenomena occurring within the AT-type precalciner, allowing for the determination of optimal SRF fuel inlet parameters while ensuring clinker quality and process efficiency.

MATERIALS AND METHODS

The methodology of the research carried out consists of many elements related to the selection of material, preparation of geometry, development of boundary and initial conditions, selection of components of the computational model.

SRF characterization

The morphological composition of SRF consists of plastics (50%), textiles (24%), and fine fraction (<0.5 mm) (26%). The properties of SRF are presented in **Table 1**.

Due to the combustion process occurring in the precalciner, it is necessary to know the fractional composition of the fuel, where each fraction is defined by its physical and thermochemical properties. Additionally, geometric parameters such as particle shape and size distribution are determined.

Table 1. Composition and properties of SRF

Parameter	Unit	SRF
$\text{Moisture}_{\text{w.b.}}$	%	9.0±2.4
$\text{Volatile Matter}_{\text{d.b.}}$	%	71.3±0.6
$\text{Ash}_{\text{d.b.}}$	%	13.3±1.1
Lower Heating Value	kJ/kg	25 891±1 398
$\text{Carbon}_{\text{d.b.}}$	%	51.1± 0.16
$\text{Hydrogen}_{\text{d.b.}}$	%	8.07 ±0.82
$\text{Nitrogen}_{\text{d.b.}}$	%	1.55 ±0.16
$\text{Suphur}_{\text{d.b.}}$	%	<0.049
$\text{Oxygen}_{\text{diff..}}$	%	39.23±0.40

w.b. – wet basis, d.b. – dry basis, diff. – calculated as a difference

Cement kiln installation

This study was conducted for an actual facility utilizing the dry method of clinker production, which features a production line with a nominal capacity of 2,800 tons per day. The primary element of the production line is a rotary kiln (ϕ 5 × 95.6 m), equipped with IV-stage cyclone preheater with an AT-type precalciner and an IKN Pendulum grate cooler. **Figure 1** illustrates the rotary kiln, with the designated research area indicated. In the precalciner, both hard coal and coal shale are burned, which serve a dual purpose in the process - as fuel and as part of the raw material set (referred to as low-grade raw material).

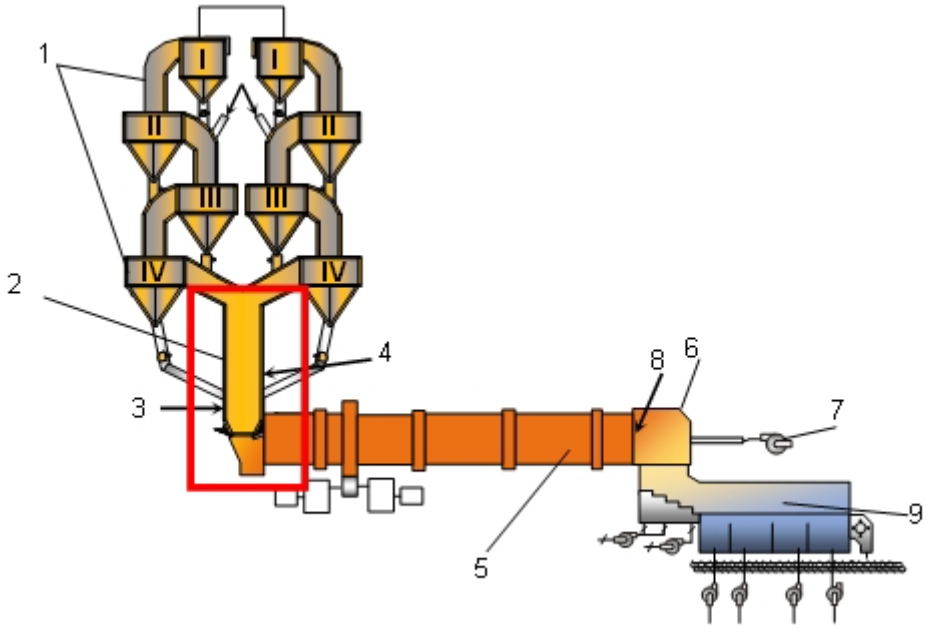

Figure 1. Scheme of cement rotary kiln: 1- preheater tower, 2 – AT preheater (AT-type precalciner), 3 – tertiary air, 4 – inlet of SRF, 5 – cement kiln, 6 – kiln head, 7 - primary air, 8 – secondary air, 9 – cooler

Coal with a calorific value of 25.6 MJ/kg is burned in the form of dust at a rate of 1000 kg/h in the precalciner. In the calculation, it is assumed that the coal burned in AT-type precalciner is 100% replaced by SRF.

Boundary conditions of calculation

For numerical calculation, a computational geometry was prepared including the design details of the AT-type precalciner along with the location of the fuel and raw material inlets (**Figure 2a**).

The analysis of operational data allowed for the adopted boundary conditions for which the calculations were carried out, as summarized in **Table 2**.

Table 2. Boundary conditions for inlet and outlet cross-sections

Cross-section	v, m/s	T, K	p_n, Pa
Inlet from kiln	15	1 273	-400
Outlet to bypass	-30	1 100	-400
Outlet to preheater tower	Calculated from the balance of the inflowing mass	1 112	-800
Raw material inlet from cyclones III	Based on the raw material stream	1 000	0
Raw material inlet from cyclones IV	Based on the raw material stream	1 100	0

Positive velocity values mean the stream inlet to the calculation region, while negative values appear in the outlet cross-sections. The list includes velocity, temperature, and gauge pressure in individual sections, the values of which were determined based on available technological data.

The research was conducted in several stages, initially determining the SRF fuel inlet diameter (150 mm), fuel flow rate (1000 kg/h), and transport air flow rate (1000 Nm^3/h). In the next stage, a simulation was conducted to assess the impact of the inlet position on the calcination process.

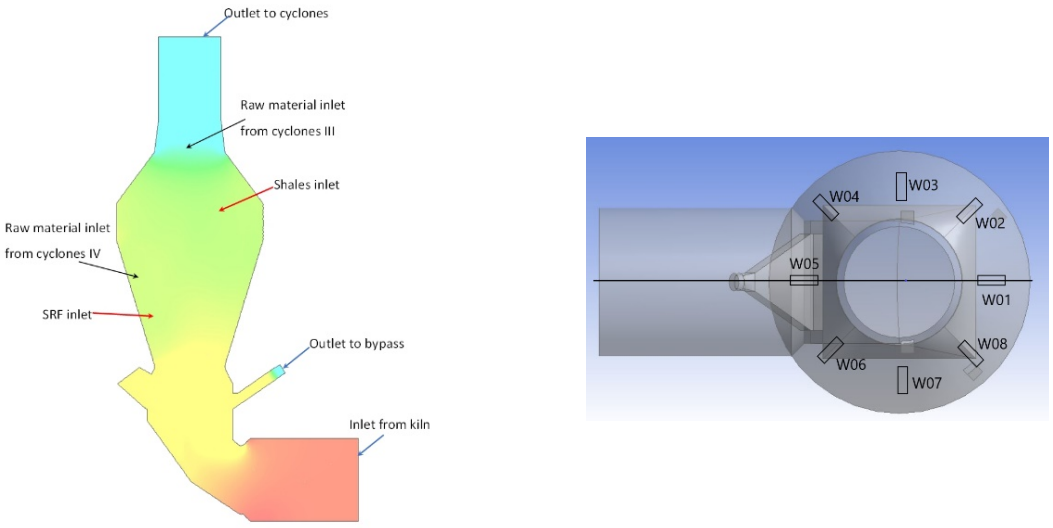

a) b)

Figure 2. Computational geometry:
a) the designation of boundary sections, b) the examined inlets of SRF fuel

The study of flow processes in various geometrical systems requires the construction of computational geometry, the determination of boundary and initial conditions, and the calculation cycle. In various works, the authors describe the calculation method, in which the first stage is usually the preparation of computational geometry. The next step is to create a computational mesh, for which its resolution is very important. A balance must be found between the accuracy of the results and the time required to obtain them [22]. In paper [23], an analysis of the influence of the grid size on the accuracy of calculations for 8 computational grids with different resolutions was carried out. The authors indicated the structured grid with 800 k cells as optimal.

The conducted research focused on determining the location of SRF inlet to the AT-type precalcinator and the methodology involved precisely identifying the inlet location, considering one level, which resulted from previously conducted preliminary research. Eight inlet variants (W01-W08) at this level were examined, differing in position, with each subsequent inlet located at an angular distance of 45 degrees. The localization of the variants is presented in **Figure 2b**.

Numerical calculation

Numerical calculation was made using the ANSYS 2020-R1 system with the FLUENT program, expanded with own procedures that implement the required assumptions. It was also necessary to create non-standard procedures related to system startup, computing server settings and data acquisition.

For the purposes of the research, a mathematical model was developed, based on the Euler method to describe the motion of the gas phase and the Lagrange method to describe the motion of particles [24]. It was assumed that the following factors influence on the process:

- flue gas flow from the rotary kiln through the AT-type precalciner,
- heat exchange between raw material particles and exhaust gases,
- combustion of additional fuel in the AT-type precalciner,
- calcination of raw material particles.

To calculate the flow field, continuity equations, momentum conservation equations, energy conservation equations, and component transportation equations were used. The coupling processing of the velocity and pressure fields in the AT-type precalciner adopted the SIMPLEC algorithm [25]. The vortex dissipation model was used for SRF particles combustion, the Standard k-ε was used for the gas-phase turbulence model [26], the discrete-phase model was chosen for the gas-solid two-phase flow [27], [28], and the P1 radiation model was used for the gas-phase radiative heat transfer [29], [30].

To realize numerical tests, the mathematical model containing equations of motion for the gaseous phase and coal dust particles was applied. The air motion was described with the Euler method, and the particle motion – by the Lagrange method. It is possible to analyze motion of the gas-particle polydispersive mixture, in this study the Particle Source In Cell (PSICell) method was applied.

Neglecting the phase changes and assuming that both phases are incompressible, and the flow is isothermic and stationary, the gas motion can be described in the uniform, generalized conservative form, isolating convection, diffusion and source components. In a consequence authors obtain [31]:

$$\frac{\partial(\rho\varphi)}{\partial t}+\frac{\partial(\rho U_{\mathrm{i}}\varphi)}{\partial x_{\mathrm{i}}}=\frac{\partial}{\partial x_{\mathrm{i}}}\left(\Gamma_{\varphi}\frac{\partial\varphi}{\partial x_{\mathrm{i}}}\right)+S_{\varphi}+S_{\varphi\mathrm{p}} \tag{1}$$

where φ is a generalized dependent variable, Γ_{φ} is the coefficient of diffusion transport, and the source term S_{φ} contains all the remaining components of the differential equations (except for convection and diffusion ones). The coefficients Γ_{φ} and S_{φ} are dependent on the variable φ and presented in **Table 3**.

The particle trajectory should be known during calculation of the mentioned above source components. The particle trajectory is calculated according to its equation of motion. If the phase density difference is big, the equation of particle motion can be written [32], [33] as:

$$m_{\mathrm{p}}\frac{du_{\mathrm{p}}}{dt}=\frac{3}{4}C_{\mathrm{D}}\frac{\rho m_{\mathrm{P}}}{\rho_{\mathrm{p}}d_{\mathrm{k}}}u\left|u-u_{\mathrm{p}}\right|\left(u-u_{\mathrm{p}}\right)+g \tag{2}$$

Conversion of momentum between the diluted and continuous phase is described by the source term:

$$\overline{S_{u_{\mathrm{i}},\mathrm{p}}}=\frac{1}{V_{\mathrm{E}}}\eta_{\mathrm{j}}\int_{\delta t_{\mathrm{j}}}\frac{\mu_{\mathrm{D}}\,Re_{\mathrm{p}}\,D_{\mathrm{p}}}{8\pi}\left(\bar{u}_{\mathrm{i}}-u_{\mathrm{pi}}\right)dt \tag{3}$$

where V_{E} is the elementary cell volume and η_{j} describe the number of particles transported at j-trajectory in the time unit, C_{d} is drag force coefficient, Re_{p} is the Reynolds number, D_{p} is particle diameter, $\overline{u_{\mathrm{i}}}$ is gas velocity, u_{p} is particle velocity.

Table 3. Coefficients of equation (1) [31]

Equation	φ	Γ_φ	S_φ	$S_{\varphi p}$
Continuity	1	0	0	0
Momentum in direction of axe x_i	u_i	μ_{ef}	$F_i - \frac{\partial p}{\partial x_i} + \frac{\partial}{\partial x_j}\left(\mu_{ef}\frac{\partial u_j}{\partial x_i}\right)$	$\overline{S_{u_i,p}}$
Kinetic turbulent energy	k	$\frac{\mu_{ef}}{\sigma_\varepsilon}$	G_k - $\rho\varepsilon$	0
Dissipation of kinetic turbulent energy	ε	$\frac{\mu_{ef}}{\sigma_\varepsilon}$	$\frac{\varepsilon}{k}(C_1 G_k - C_2\rho\varepsilon)$	0
Energy	E	$\frac{\lambda_{ef}}{c_p}$	ρS_E	S_{E_p}

$$G_k = \frac{\partial u_i}{\partial x_j}\mu_t\left(\frac{\partial u_i}{\partial x_j} + \frac{\partial u_j}{\partial x_i}\right);\ \mu_{ef} = \mu + \mu_t;\ \mu_t = C_\mu\rho\frac{k^2}{\varepsilon}$$

C_μ=0,09; C_1=1,44; C_2=1,92; σ_k=1,0; σ_ε=1,3;

The particle motion trajectories were obtained by integrating eq. (3) in the gas phase velocity field. In the Lagrange method, the particles are delivered to the system with a finite number of discrete point inlets. The study takes into account the polydispersity of particles, both in the case of raw material and railroad tie particles.

The particle-wall collision model can be selected experimentally or can be based on the particle-wall collision equations. The first method requires a large number of experiments and is not universal, while the second method is applicable to a larger number of issues and is currently preferred. The coefficient of restitution is highly dependent on the coefficient of kinetic friction, the particle velocity, the angle of incidence, and the material properties of the particle and the wall. Experimental studies show that the coefficient of restitution is highly dependent on the smoothness of the wall surface and the shape of the particle. Taking into account the boundary condition on the wall: trap or reflect significantly affects the behavior of the particles [34].

Boundary and initial conditions appropriate for all variables are attached to the system of equations. Particular equations are interconnected, which forces to use special numerical techniques to solve them. The developed mathematical model allows to determine the exchange of fuel and gas phase components through surface exchange, as well as to calculate heat fluxes.

The actual processes occurring in the AT-type precalciner are complicated and it is difficult to verify the calculation results with the experimental data. Therefore, it is advisable to develop a simple, efficient tool that will allow to consider the main effects, indicate process change trends, and allows particulate matter to be included in local energy balances.

Modeling the fuel combustion process

The most significant physicochemical change affecting fuel particles during their heating is thermal fragmentation (pyrolysis) at high temperature. At this stage, significant weight loss occurs as a result of the release of volatile components, the quantitative and qualitative composition of which depends on the fuel components, their size and temperature. During the release of components, a number of parallel chemical reactions occur, which involve combinations of reacting components such as CH_4, CHOH, C_2H_6, H_2 and S_2. After the release of components directed to the production of water vapor, CO, CO_2, etc., a series of gradual carbonization reactions and gas release takes place according to the following scheme.

Heterogeneous reactions:

$$\begin{aligned} &C_{(s)} + O_{2(g)} \Rightarrow CO_{2(g)} \\ &2C_{(s)} + O_{2(g)} \Rightarrow 2CO_{(g)} \\ &C_{(s)} + 2H_{2(g)} \Rightarrow CH_{4(g)} \\ &C_{(s)} + CO_{2(g)} \Rightarrow 2CO_{(g)} \\ &C_{(s)} + H_2O_{(g)} \Rightarrow CO_{(g)} + H_{2(g)} \end{aligned} \quad (4)$$

Homogeneous reactions:

$$\begin{aligned} &2CO_{(g)} + O_{2(g)} \Rightarrow 2CO_{2(g)} \\ &CO_{(g)} + H_2O_{(g)} \Rightarrow CO_{2(g)} + H_{2(g)} \\ &CO_{(g)} + 3H_{2(g)} \Rightarrow CH_{4(g)} + H_2O_{(g)} \\ &CH_{4(g)} + 2O_{2(g)} \Rightarrow CO_{2(g)} + H_2O_{(g)} \\ &HC_{(g)} + 1.5O_{2(g)} \Rightarrow CO_{2(g)} + H_2O_{(g)} \end{aligned} \quad (5)$$

The model also includes decomposition and polymerization reactions of saturated and unsaturated hydrocarbons:

$$\begin{aligned} &\text{High} \quad HC_{(g)} \xrightarrow{\text{fragmentation}} \text{Low} \quad HC_{(g)} + C_{(s)} \\ &\text{Unsaturated} \quad HC_{(g)} \longrightarrow \text{Saturated} \quad HC_{(g)} \\ &\text{Unsaturated} \quad HC_{(g)} + H_{2(g)} \xrightarrow{\text{polymerization}} \text{High} \quad HC_{(g)} \end{aligned} \quad (6)$$

As the temperature increases, moisture and gaseous components contained in the fuel are released. Percentage more chemically free water evaporates at temperatures below 105 °C, while chemically bound water evaporates at temperatures above 350 °C. At the pyrolysis temperature, some types of fuel melt, forming a transitional product called metaplast. As the temperature increases, the metaplast separates to form basic volatile components, while an increase in particle volume is observed for the solid residue. The increase in particle volume does not affect the pyrolysis rate, but the particles decompose. The decomposition rate increases with increasing temperature until it reaches a maximum value. The end of the pyrolysis process occurs at temperatures of 850 – 1000 °C, while its duration is limited to a few seconds, depending on the particle size. After the gaseous components are released, the remaining solids (degassed) still retain small amounts of them. Components such as H_2 and N_2 may be present in these conditions in amounts up to approx. 1.5%, and after exceeding the temperature of 2000 °C, they are released completely. The solid particle residues after the release of gaseous components are composed mainly of carbon with high porosity and internal surface and inorganic ash. Temperatures in the range of 1200 – 1800 °C cause the ash to melt. The composition and nature of the ash, as well as its properties, depend largely on the pyrolysis conditions.

When the gas phase contains mainly air, pyrolysis and combustion of carbonized particles occur simultaneously, pyrolysis precedes combustion by a very small-time step. In ordinary fuel particles, gaseous components are released from the surface in concentrated but random streams. When the gas phase is hot enough and rich in oxygen, the streams of released gases form a flame. For relatively large particles, the release and combustion of gaseous components can render the zone just at the surface of the particle free of oxygen. When oxygen flows to the

surface of hot carbonized particles, a heterogeneous combustion reaction will occur with a duration 15-20 times longer than the thermal decomposition time of the particle.

The heating rate of fuel particles depends on their size and contact with the heat source. When heated, components are released, which mainly include CO, CH, H_2O and H_2. Assuming that there is an oxidant in the calciner chamber and assuming that all these components react with the oxidant, the main reactions that take place in the system under study are:

$$\begin{aligned} &CO + 1/2O_2 \rightarrow CO_2 - 283.2\text{kJ/mol} \\ &H_2 + 1/2O_2 \rightarrow H_2O - 242\text{kJ/mol} \\ &CH_4 + 2O_2 \rightarrow CO_2 + 2H_2O - 802.86\text{kJ/mol} \end{aligned} \tag{7}$$

Model of particulate degassing

The particle outgassing model can be presented in the form of the following equations:

$$R_1 = A_1 \exp\left(\frac{E_1}{RT_\text{p}}\right) \tag{8}$$

$$R_2 = A_2 \exp\left(\frac{E_2}{RT_\text{p}}\right) \tag{9}$$

where R_1 and R_2 are reaction rate constants used interchangeably in different temperature ranges. They allow for the introduction of an equation defining outgassing in the following form:

$$\frac{m_\text{v}(t)}{m_\text{po} - m_\text{ash}} = \int_0^t (a_1 R_1 + a_2 R_2) exp\left(\int_0^t (R_1 + R_2) dt\right) dt \tag{10}$$

where: A is the constant for a given reaction, also called the pre-exponential factor, R (universal) gas constant and T is the temperature. There is therefore a direct relationship between the activation energy and the reaction rate: the smaller E_a, the higher the reaction rate.

The degassing model requires knowledge of the kinetic parameters (A_1, E_1) and (A_2, E_2) and the contributions of two reactions through the factors a_1 and a_2. More specifically, A_1=2.0e+07 s^{-1}, A_2=1.0e+07 s^{-1} denote the pre-exponential factors and E_1=1.04e+05 J/mol and E_2=1.67e+05 J/mol denote the activation energy of the reaction. Activation energy - is the value of the energy barrier (on a microscopic scale - the potential barrier), which is often given per 1 mole of substance, which the system of reacting chemical entities must overcome in order for a chemical reaction to occur.

Combustion of carbonized particles

The reactions of fuel particles with oxygen are described by two mathematical models: single layer and double layer. In the first model, oxygen diffuses through the solid boundary layer to the surface of the carbonized particle, where it reacts to CO and CO_2. The CO then diffuses into the surroundings. In the second model, the carbonized particles react with CO_2 rather than oxygen, producing CO, which is burned in a thin flame inside the boundary layer. CO reacts with oxygen inside the boundary layer, which prevents oxygen from reaching the surface of the particle. The combustion of particles smaller than 100 μm is modeled by the first method, and those larger than 2 mm by the second.

The actual combustion mechanism is more complicated because there are many factors involved such as particle size, local temperature, local oxygen concentration. In general, oxygen and CO are readily available on the carbon surface and can therefore react simultaneously with the carbon contained in the particles and with each other.

Model of surface particle combustion

After degassing the fuel particles, a chemical reaction begins on the particle surface, which is modeled using the diffusion or kinetic-diffusion method.

Diffusion model. The reaction rate is determined by the diffusion of the oxidant towards the surface of the carbon particle, which is determined by the following equation:

$$\frac{dm_{\mathrm{p}}}{dt} = -4\pi D_{\mathrm{p}} D_{\mathrm{i,m}} \frac{m_0 T_{\mathrm{p}} \rho_{\mathrm{g}}}{S_{\mathrm{b}}\left(T_{\mathrm{p}} + T_{\infty}\right)} \tag{11}$$

where $D_{\mathrm{i,m}}$ is the diffusion coefficient of the oxidant, S_{b} is the stoichiometric component (the ratio of the mass of the oxidant to the mass of the oxidized particle), m_0 is the local mass fraction of the oxidant in the gaseous environment, and T_{p} and T_{∞} are the temperature of the particle and its gaseous surroundings, respectively.

In this model, it is assumed that the particle diameter is constant and its mass decreases as the reaction progresses. The active density decreases, which increases the porosity of the particle. This model neglects the contribution of kinetics to the surface reaction.

Kinetic-diffusion model. The reaction rate is determined by the diffusion of the oxidant towards the surface of the fuel particle or the reaction kinetics. In this model, the rate of diffusion determines the relationship:

$$R_1 = A_1 \frac{\left[\left(T_{\mathrm{p}} + T_{\infty}\right)/2\right]^{0.75}}{D_{\mathrm{p}}} \tag{12}$$

and the rate of a chemical reaction is as follows:

$$R_2 = A_2 \exp\left(-\frac{E}{RT_{\mathrm{p}}}\right) \tag{13}$$

The rate of reaction kinetics takes into account the effects of chemical reactions taking place on the inner surfaces of fuel particles and diffusion into the particle. The rates R_1 and R_2 are related by an equation defining the rate of combustion of fuel particles in the following form:

$$\frac{dm_{\mathrm{p}}}{dt} = -\pi D_{\mathrm{p}}^2 \frac{R_1 R_2}{R_1 + R_2} \tag{14}$$

The particle size is held constant until the mass reduction exceeds a level, at which point a new particle size is estimated.

Modeling of the calcination process of clinker meal particles

During the movement of limestone particles through the calciner chamber, five stages of the calcination process accompanying this movement can be distinguished:

1. In the preheating zone, the limestone is heated from ambient temperature to approximately 800 °C by hot gases (e.g., combustion products, CO_2 from the calcination process and additional air).
2. From approximately 800 °C, the pressure of carbon dioxide produced as a result of limestone dissociation becomes equal to the partial pressure of CO_2 in the gases of the precalciner chamber.
3. When the temperature of limestone exceeds 900 °C, i.e. the decomposition temperature, and the partial pressure exceeds 1 atmosphere, the dissociation process may proceed from the surface towards the center of the particles.
4. If all the calcium carbonate contained in the particles dissociates before the particles leave the calcination zone, the lime begins to sinter.
5. Lime particles that may contain limestone residues leave the calcination zone and are cooled by the air supplied for combustion.

The reaction of thermal decomposition of calcium carbonate can be written as follows:

$$\begin{aligned} &CaCO_3 + \xrightarrow{178\text{kJ/kg}} CaO + CO_2 \uparrow \\ &100\text{g} \xrightarrow{\cdots\cdots\cdots\cdots} 56\text{g} + \quad 44\text{g} \end{aligned} \tag{15}$$

The shrinking core model was adopted to study the distribution of spherical limestone particles during the calcination process. At a given time step, there is a centrally located core of undecomposed carbonate surrounded by a calcium oxide shell with the reaction front occurring on the surface between the core and the shell.

On the reaction surface, the mass equilibrium for the calcining material can be written in the following form:

$$\frac{dm_{\text{p.L}}}{dt} = -r_{\text{c}} \frac{Mw_{CO_2}}{Mw_{CaCO_3}} \tag{16}$$

where

$$r_{\text{c}} = \ {}^{\text{r}}k'_{\text{s}} \times \text{e}^{-E_2/RT_{\text{L}}} \times 4\pi \times r_{\text{p}}^2 \times Mw_{CaCO_3} \tag{17}$$

while $m_{\text{p,L}}$, Mw_{CO2}, Mw_{CaCO3} are the mass of the reacting limestone particle, the atomic mass of carbon dioxide and calcium carbonate. r_{c} is the calcination coefficient of calcium carbonate and r_{p} is the shrinking radius of the uncalcined part of the particle. The ${}^{\text{r}}k'_{\text{s}}$ value is calculated from the relationship:

$$\begin{aligned} {}^{\text{r}}k'_{\text{s}} &= {}^{\text{r}}k_{\text{s}} \quad \text{for} \quad p_{CO_2} < 10^{-2} p_{\text{eq}} \\ {}^{\text{r}}k'_{\text{s}} &= {}^{\text{r}}k_{\text{s}} \left(\frac{p_{CO_2} - p_{\text{eq}}}{p_{\text{eq}}} \right) \quad \text{for} \quad 10^{-2} p_{\text{eq}} < p_{CO_2} < p_{\text{eq}} \end{aligned} \tag{18}$$

where

$$p_{\text{eq}} = 1.826 \times 10^7 \exp\left(-\frac{19680}{T_{\text{L}}} \right) \tag{19}$$

The ${}^{r}k_{s}$ component is the calcination constant of calcium carbonate, while T_{L} is the temperature of the $CaCO_3$ particle. The presence of CO_2 in ambient gases inhibits the calcination process, but it is difficult to determine the influence of the partial pressure exerted by CO_2 on this process. $CaCO_3$ particle calcination model is presented in **Figure 3**.

The energy balance for the calcareous uncalcined core of the particle can be written as follows:

$$\frac{d\left(m_{p,L}C_{p,s}T_{L}\right)}{dt} = h_{c,L}\ {}^{L}A_{p}\left(T_{g}-T_{L}\right) + \sigma\varepsilon_{L}\ {}^{L}A_{p}\left(T_{g}^{4}-T_{L}^{4}\right) + C_{p,s}T_{L}\frac{dm_{p,L}}{dt} \tag{20}$$

where T_{L} is the temperature of the particle core, ε_{L} is the emissivity of the particle, ${}^{L}A_{P}$ is the external field of the particle core.

The above calcination model can also be presented in the form of the calcination degree, which is information about the amount of carbon dioxide released from the particle in relation to the potential amount of this gas in the particle. The degree of calcination α is described by the following equation:

$$1-(1-\alpha)^{\frac{1}{3}} = \frac{{}^{r}k_{s}'}{D_{p}}\exp\left(-\frac{E}{RT_{L}}\right)\frac{P_{eq}-P}{P_{eq}}t \tag{21}$$

where

$$\lg\left(P_{eq}\right) = -\frac{9300}{T} + 6.86 \tag{22}$$

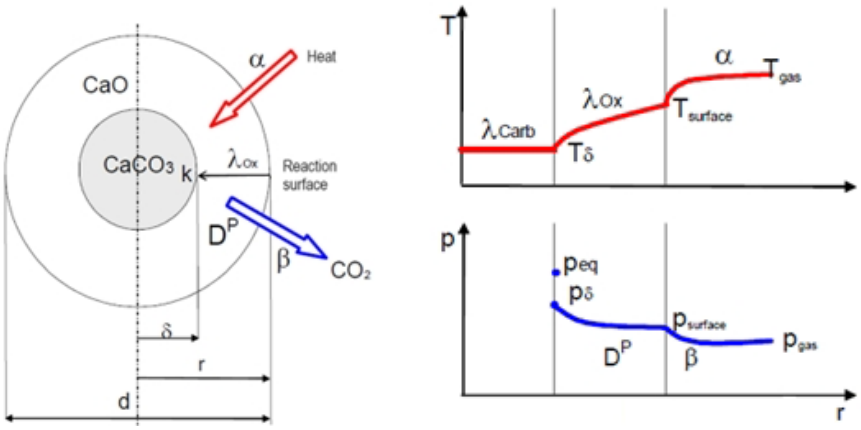

Figure 3. $CaCO_3$ parcitle calcination model:
a) temperature and pressure distributions in the volume of the particle,
b) calcination mechanism

Calculation methodology

In order to obtain calculation results for the gas and solid phases, it is necessary to properly define the investigated problem in terms of the use of available numerical techniques for its implementation. The initial stage is the discretization of the computational area into a finite number of unit cells. The next step is to present the differential equations in discrete form and set appropriate conditions on the edges of the discretized computational grid. After preparing the issue under consideration for numerical calculations, an iterative process of searching for a solution takes place.

The iterative algorithm for numerical simulation of the flow of two phases with bilateral coupling is as follows:

1. Preliminary calculation of the gas velocity field without taking into account the source components $S_{\Phi p}$ coming from the fragmented phase in the solution (Eulerian stage),
2. Calculation of trajectories for a large number of particles moving in the gas velocity field with simultaneous calculation of source components $S_{\Phi p}$ (Lagrange stage),
3. Recalculation of the velocity fields taking into account the source factors of the fragmented phase $S_{\Phi p}$,
4. Repeating steps 2 and 3 until the equations for the coupled phases converge.

For the flow of a fluid containing solid particles with one-sided coupling, the calculation cycle is limited to the first two steps of the iterative algorithm.

The calculation procedure for the Lagrange phase is as follows:

- separating a finite number of point inlets in the control cross-section (inlet to the system), through which particles of individual fractions with a known mass fraction are delivered,
- determination of particle trajectories for all point inlets,
- determining the points of collision of particles with walls,
- determining the effects of combustion on fuel particles,
- determination of the degree of calcination for $CaCO_3$ particles,
- calculation of the source terms $S_{\phi p}$ in the equations for gas components,
- calculation of the concentration of nitrogen oxides in the gas mixture.

RESULTS AND DISCUSSION

In the developed mathematical model, it is possible to precisely determine the temperature in each cell, enabling the identification of regions where the calcination process occurs more rapidly. This means that areas with higher temperatures will facilitate a more dynamic progression of this process. **Figure 4** depict these regions where the temperature ranges from 1100 to 1300 K, allowing for the identification of locations where calcination may occur most efficiently.

Based on the conducted analyses, it is evident that variant W-04 offers the most extensive region within the temperature range of 1100 to 1300 K, potentially positively impacting the calcination process.

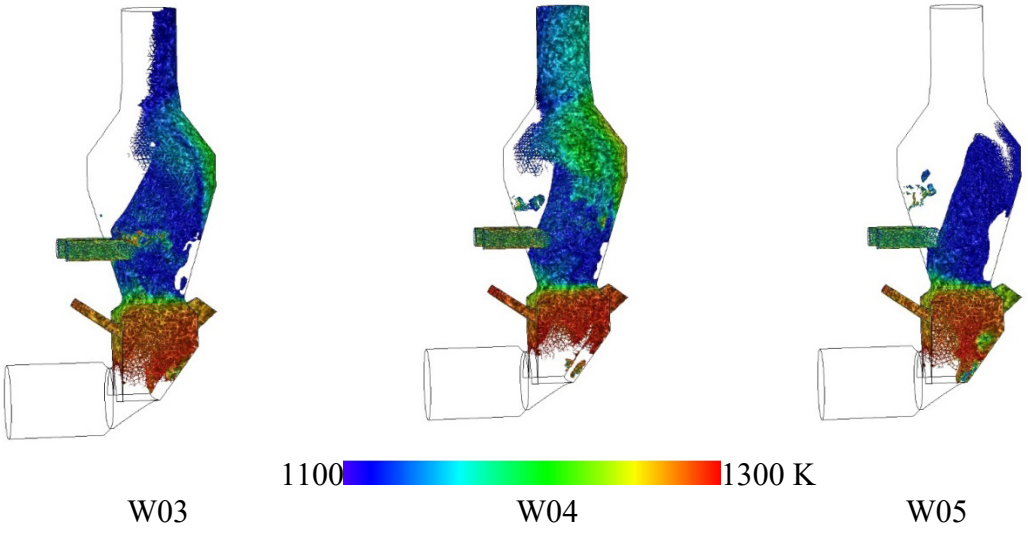

Figure 4. Temperature profile of the gas phase in calculation domain (1100-1300 K) for selected variants

The obtained data allow for the identification of regions with specific values of the mole fractions of gaseous components such as CO, CO_2, O_2. Carbon dioxide is emitted during the calcination process, which is facilitated in zones where the mole fraction of this component is as low as possible [9]. **Figure 5** illustrates regions with a CO_2 mole fraction ranging from 0 to 0.2.

An essential element influencing the calcination process is the concentration of CO_2 surrounding the particle. It is preferable for this concentration to be minimized. This preference arises from the fact that a reduced partial pressure of CO_2 accelerates the calcination kinetics [10]. Comparing the variants presented in **Figure 5**, it can be observed that in the case of variant W-04, the region with a CO_2 mole fraction within the range of 0.2 is the largest.

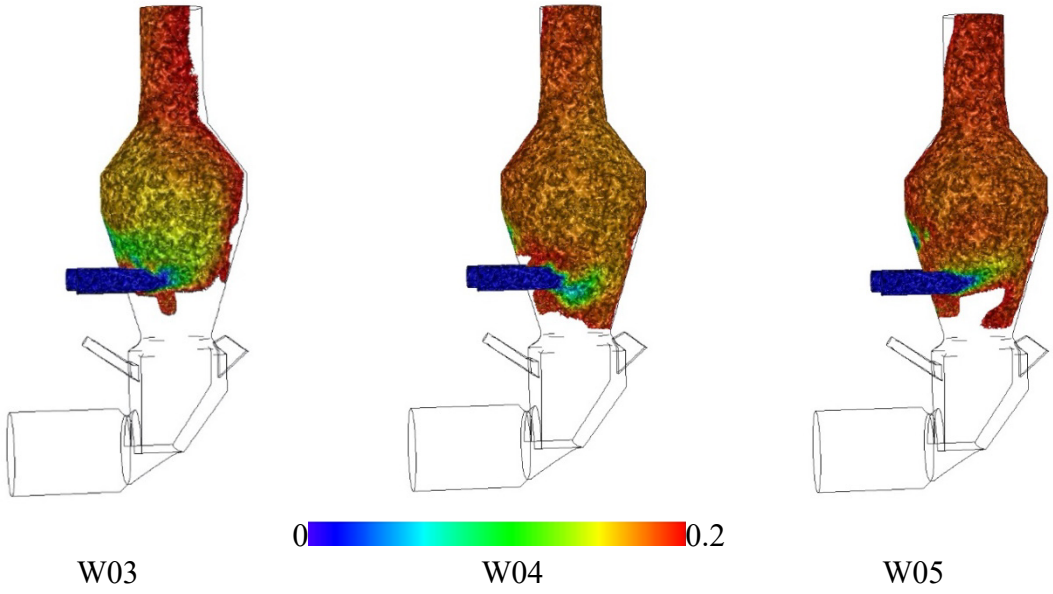

Figure 5. Profiles with CO_2 mole fractions ranging from 0 to 0.2 for selected variants

The research was carried out to determine the optimal location of the alternative fuel inlet, at which, at the outlet from the AT-type precalciner, the mole fraction of CO and CO_2 will be the lowest.

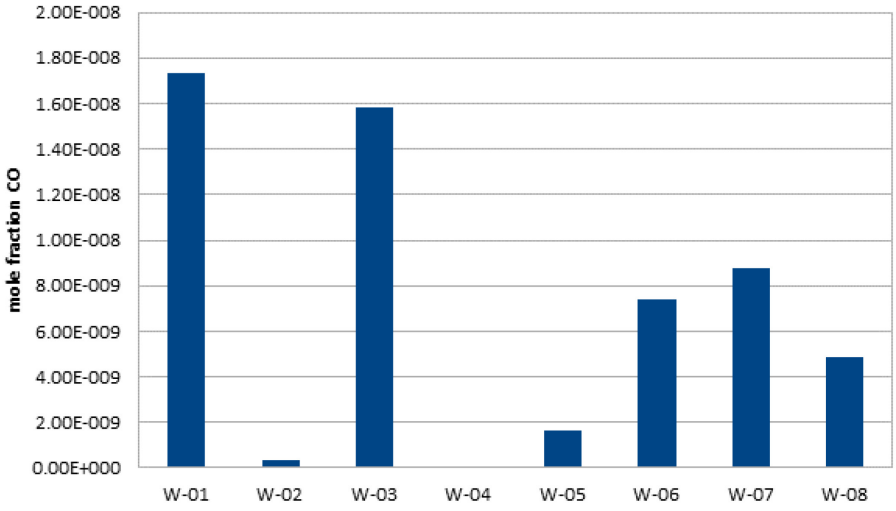

Figure 6. Mole fraction of CO at outlet from AT-type precalciner

Figure 6 and **Figure 7** present mole fractions at the outlet from the AT-type precalciner.

Figure 7. Mole fraction of CO_2 at outlet from AT-type precalciner

It is evident that values diverge depending on the SRF fuel inlet position. In the case of variant W-04, the CO mole fraction at the AT-type precalciner outlet is the lowest, measuring 4.35E-13, while the CO_2 mole fraction stands at 0.191.

Based on these findings, it can be inferred that the optimal location for installing the SRF fuel inlet is variant W-04.

CONCLUSION

The analysis was conducted to determine the optimal location of the alternative fuel inlet, which affects the minimization of the mole fractions of CO and CO_2 at the outlet from the AT-type precalciner. The obtained results indicated that variant 4 (W-O4), based on the adopted criteria, best fulfills the conditions necessary for conducting the calcination process because:

- it demonstrates the most extensive region within the temperature range of 1100 to 1300 K, which could positively impact the calcination process,
- it exhibits the largest region with a CO_2 mole fraction within the desired range of 0.2. Minimizing the concentration of CO_2 surrounding the particle is crucial for enhancing calcination kinetics,
- the CO mole fraction at the precalciner outlet is the lowest at $0.435 \cdot 10^{-12}$, with a CO_2 mole fraction of 0.191.

Furthermore, the following conclusions were drawn based on the motion of fuel particles:

- the movement of fuel particles is determined by the velocity distribution in the analyzed geometry,
- to maintain conditions that achieve similar free-fall velocities of the particles, it is insufficient to preserve only the geometric similarity of the system. Dynamic similarity should also be maintained. This implies that adapting the obtained results to other systems with significantly different shapes or geometries is impossible without conducting appropriate studies for each of these systems,
- the proposed methodology is suitable for any geometry; however, for similar installations applied in other cement plants, the results can be adapted with shape corrections to account for geometric differences.

ACKNOWLEDGMENT

The authors would like to acknowledge the financial support provided the Polish Minister of Higher Education under the *'Regional Initiative of Excellence Program'* project RID/SP/0041/2024/01

REFERENCES

1. A. Talaei, D. Pier, A. V. Iyer, M. Ahiduzzaman, and A. Kumar, "Assessment of long-term energy efficiency improvement and greenhouse gas emissions mitigation options for the cement industry," *Energy*, vol. 170, pp. 1051–1066, Mar. 2019, https://doi.org/10.1016/j.energy.2018.12.088.
2. "2024 Guide: The Cement Industry in Figures," *Polish Cement Association*, 2024. https://www.polskicement.pl/2024-informator-spc-przemysl-cementowy-w-liczbach, [Accessed: Mar. 19, 2025].
3. "Key Facts & Figures," *CEMBUREAU*, 2024. https://www.cembureau.eu/media/00ejjcfj/key-facts-figures-publication-june-2024.pdf, [Accessed: Mar. 19, 2025].
4. "CEN/TC 343 Solid Recovered Fuels," *European Committee for Standardization*, 2022. https://standards.cencenelec.eu/BPCEN/407430.pdf, [Accessed: Mar. 19, 2025].
5. C. Pieper, B. Liedmann, S. Wirtz, V. Scherer, N. Bodendiek, and S. Schaefer, "Interaction of the combustion of refuse derived fuel with the clinker bed in rotary cement kilns: A numerical study," *Fuel*, vol. 266, p. 117048, Apr. 2020, https://doi.org/10.1016/j.fuel.2020.117048.
6. N. Chatziaras, C. S. Psomopoulos, and N. J. Themelis, "Use of waste derived fuels in cement industry: a review," *Management of Environmental Quality: An International Journal*. 2016, https://doi.org/10.1108/MEQ-01-2015-0012.
7. R. Junga, M. Wzorek, and M. Kaszubska, "Technical and environmental performance of 10 kW understocker boiler during combustion of biomass and conventional fuels," *E3S Web Conf.*, vol. 19, p. 01009, Oct. 2017, https://doi.org/10.1051/e3sconf/20171901009.
8. M. Wzorek, M., Baran, T., Ostrowski, "The influence of fly ash absorption from secondary fuels combustion on clinkering process and hydraulic activity of Portland cement clinker," *Cem. Wapno Bet.*, vol. 4, pp. 207–215, 2013.
9. K. T. Kaddatz, M. G. Rasul, and A. Rahman, "Alternative fuels for use in cement kilns: Process impact modelling," 2013, https://doi.org/10.1016/j.proeng.2013.03.141.
10. Z. Kang, F. Su, L. Fang, and H. Zhu, "DEM-CFD coupled simulation of limestone calcination and fuel combustion in beam type lime shaft kiln," *Appl. Therm. Eng.*, vol. 231, p. 120935, Aug. 2023, https://doi.org/10.1016/j.applthermaleng.2023.120935.
11. W. Wang, Y. Liao, J. Liu, Z. Huang, and M. Tian, "Numerical Simulation and Optimization of Staged Combustion and NOx Release Characteristics in Precalciner," *J. Therm. Sci.*, vol. 28, no. 5, pp. 1024–1034, Oct. 2019, https://doi.org/10.1007/s11630-019-1164-y.
12. B.-J. R. Mungyeko Bisulandu and F. Marias, "Modeling of the Thermochemical Conversion of Biomass in Cement Rotary Kiln," *Waste and Biomass Valorization*, vol. 12, no. 2, pp. 1005–1024, Feb. 2021, https://doi.org/10.1007/s12649-020-01001-9.
13. J. Hercog *et al.*, "Pilot testing and numerical simulations of the multifuel burner for the cement kiln," *Fuel*, vol. 342, p. 127801, Jun. 2023, https://doi.org/10.1016/J.FUEL.2023.127801.
14. W. K. H. Ariyaratne, A. Malagalage, M. C. Melaaen, and L.-A. Tokheim, "CFD modelling of meat and bone meal combustion in a cement rotary kiln – Investigation of fuel particle size and fuel feeding position impacts," *Chem. Eng. Sci.*, vol. 123, pp. 596–608, Feb. 2015, https://doi.org/10.1016/j.ces.2014.10.048.

15. L. Chen, Z. Sun, H. Ma, G. Pan, P. Li, and K. Gao, "Flow characteristics of pneumatic conveying of stiff shotcrete based on CFD-DEM method," *Powder Technol.*, vol. 397, p. 117109, Jan. 2022, https://doi.org/10.1016/j.powtec.2022.117109.
16. L. Reineking *et al.*, "Convective drying of wood chips: Accelerating coupled DEM-CFD simulations with parametrized reduced single particle models," *Particuology*, vol. 84, pp. 158–167, Jan. 2024, https://doi.org/10.1016/j.partic.2023.03.012.
17. R. Gao, S. Yin, T. Song, and P. Lu, "Numerical simulation of co-combustion of pulverized coal and biomass in TTF precalciner," *Fuel*, vol. 334, p. 126515, Feb. 2023, https://doi.org/10.1016/j.fuel.2022.126515.
18. L. Zhang, X. Wei, Z. Zhang, and S. Li, "Modeling De-NOx by Injection Ammonia in High Temperature Zone of Cement Precalciner," *J. Therm. Sci.*, vol. 30, no. 2, pp. 636–643, Mar. 2021, https://doi.org/10.1007/s11630-020-1324-0.
19. H. Mikulčić, E. von Berg, M. Vujanović, X. Wang, H. Tan, and N. Duić, "Numerical evaluation of different pulverized coal and solid recovered fuel co-firing modes inside a large-scale cement calciner," *Appl. Energy*, vol. 184, pp. 1292–1305, Dec. 2016, https://doi.org/10.1016/j.apenergy.2016.05.012.
20. Z. Leyu, C. Qingqing, W. Xiaolin, C. Heng, and L. Sen, "Effect of raw material, moisture and high-temperature tertiary air on a coal gasifier for cement precalciation," *Fuel Process. Technol.*, vol. 262, p. 108113, Oct. 2024, https://doi.org/10.1016/j.fuproc.2024.108113.
21. Q. Zheng, Y. Tian, W. Wang, J. Ye, Q. Zheng, and S. Kuang, "CFD simulation of a cement precalciner with agglomerate-based drag modeling," *Powder Technol.*, vol. 436, p. 119508, Mar. 2024, https://doi.org/10.1016/j.powtec.2024.119508.
22. L. L. Lulbadda Waduge, S. Zigan, L. E. Stone, A. Belaidi, and P. García-Triñanes, "Predicting concentrations of fine particles in enclosed vessels using a camera based system and CFD simulations," *Process Saf. Environ. Prot.*, vol. 105, pp. 262–273, Jan. 2017, https://doi.org/10.1016/j.psep.2016.11.013.
23. S. Patronelli, M. Antonelli, L. Tognotti, and C. Galletti, "Combustion of wood-chips in a small-scale fixed-bed boiler: Validation of the numerical model through in-flame measurements," *Fuel*, vol. 221, pp. 128–137, Jun. 2018, https://doi.org/10.1016/j.fuel.2018.02.083.
24. M. Wasilewski and L. Singh Brar, "Investigations of the flow field inside a square cyclone separator using DPIV and CFD," *E3S Web Conf.*, vol. 100, p. 00083, Jun. 2019, https://doi.org/10.1051/e3sconf/201910000083.
25. M. Wang, B. Liao, Y. Liu, S. Wang, S. Qing, and A. Zhang, "Numerical simulation of oxy-coal combustion in a rotary cement kiln," *Appl. Therm. Eng.*, vol. 103, pp. 491–500, Jun. 2016, https://doi.org/10.1016/j.applthermaleng.2016.04.028.
26. J. Branco, P. J. Coelho, and M. Costa, "Experimental and numerical investigation of turbulent diffusion flames in a laboratory combustor with a slot burner," *Fuel*, vol. 175, pp. 182–190, Jul. 2016, https://doi.org/10.1016/j.fuel.2016.02.046.
27. M. A. Gómez, J. Porteiro, D. de la Cuesta, D. Patiño, and J. L. Míguez, "Numerical simulation of the combustion process of a pellet-drop-feed boiler," *Fuel*, vol. 184, pp. 987–999, Nov. 2016, https://doi.org/10.1016/j.fuel.2015.11.082.
28. B. Rahmanian, M. R. Safaei, S. N. Kazi, G. Ahmadi, H. F. Oztop, and K. Vafai, "Investigation of pollutant reduction by simulation of turbulent non-premixed pulverized coal combustion," *Appl. Therm. Eng.*, vol. 73, no. 1, pp. 1222–1235, Dec. 2014, https://doi.org/10.1016/J.APPLTHERMALENG.2014.09.016.
29. T. Kangwanpongpan, R. Corrêa da Silva, and H. J. Krautz, "Prediction of oxy-coal combustion through an optimized weighted sum of gray gases model," *Energy*, vol. 41, no. 1, pp. 244–251, May 2012, https://doi.org/10.1016/j.energy.2011.06.010.

30. K. S. Mujumdar and V. V. Ranade, "CFD modeling of rotary cement kilns," *Asia-Pacific J. Chem. Eng.*, vol. 3, no. 2, pp. 106–118, Mar. 2008, https://doi.org/10.1002/apj.123.
31. G. Borsuk, B. Dobrowolski, G. Nowosielski, J. Wydrych, and J. Duda, "Numerical simulation of thermal-hydraulic processes in the riser chamber of installation for clinker production," *Arch. Thermodyn.*, vol. 37, no. 1, pp. 127–142, Mar. 2016, https://doi.org/10.1515/aoter-2016-0009.
32. H. Mikulčić, E. von Berg, M. Vujanović, and N. Duić, "Numerical study of co-firing pulverized coal and biomass inside a cement calciner," *Waste Manag. Res. J. a Sustain. Circ. Econ.*, vol. 32, no. 7, pp. 661–669, Jul. 2014, https://doi.org/10.1177/0734242X14538309.
33. G. Borsuk, B. Dobrowolski, G. Nowosielski, J. Wydrych, and J. Duda, "Numerical simulation of thermal-hydraulic processes in the riser chamber of installation for clinker production," *Arch. Thermodyn.*, vol. 37, no. 1, 2016, https://doi.org/10.1515/aoter-2016-0009.
34. M. Bovand, S. Rashidi, G. Ahmadi, and J. A. Esfahani, "Effects of trap and reflect particle boundary conditions on particle transport and convective heat transfer for duct flow - A two-way coupling of Eulerian-Lagrangian model," *Appl. Therm. Eng.*, vol. 108, pp. 368–377, Sep. 2016, https://doi.org/10.1016/j.applthermaleng.2016.07.124.

Paper submitted: 21.11.2024
Paper revised: 19.03.2025
Paper accepted: 24.03.2025